EASR

Engineering and Applied Science Research

https://www.tci-thaijo.org/index.php/easr/index

Published by the Faculty of Engineering, Khon Kaen University, Thailand

Preparation and characterization of hydroxyapatite powder for biomedical applications from giant African land snail shell using a hydrothermal technique

Kolawole Maruf Yinka*[1)], Aweda Jacob Olayiwola[2)], Abdulkareem Sulaiman[2)], Asif Ali[3)] and Farasat Iqbal[3)]

[1)]Department of Mechanical Engineering, College of Engineering & Technology, Kwara State University, Nigeria
[2)]Department of Mechanical Engineering, Faculty of Engineering & Technology, University of Ilorin, Nigeria
[3)]Interdisciplinary Research Centre in Biomedical Materials, COMSATS University Islamabad, Lahore Campus, Pakistan

Received 6 November 2019
Revised 18 February 2020
Accepted 24 February 2020

Abstract

The need for hydroxyapatite synthesized from an inexpensive raw material is on the increase due to the expense of high purity calcium and demand of hydroxyapatite powder in dentistry, orthopaedics and trauma surgery. Additionally, efforts towards recycling and reuse of waste into value added products such as hydroxyapatite, have been one of the targeted goals of the SDG by the year 2030 to improve healthcare and for environmental friendliness. Giant African land snail shells (*Archachatina marginata*) are a waste material that is now being considered for use as a calcium precursor for hydroxyapatite production. Additionally, the effect of various low temperature hydrothermal treatments on the properties of hydroxyapatite derived in this manner are presented. Snail shell powder calcined at 900 ℃ for 3 hours in a bench top electric furnace was used in the current study as calcium precursor. Hydroxyapatite (HA) powder was prepared via a hydrothermal technique at 100, 150 and 200 ℃ for 4 hr of soaking time. Characterization of calcined and un-calcined snail shell as well as hydroxyapatite powders was done using XRF, XRD, FTIR, SEM/EDS to determine the phase content, functional groups, morphology and elemental composition, respectively. Results of calcination indicated a 81.80% CaO yield compared to 66.4% for un-calcined snail shell powder. The outcome of XRD and FTIR analyses of hydroxyapatite powders produced under various hydrothermal treatments compare favourably with HA currently available on the market. The hydrothermal temperature influenced the crystallite size and microstructure of hydroxyapatite powder. A minimum crystallite size of 23.1 nm with Ca/P stoichiometric ratio of 1.6, suitable for biomedical applications, was obtained at 100 ℃. This is compared to a crystallite size of 50.58 nm for commercial hydroxyapatite examined under the same conditions. Hence, African giant snail shells can serve as inexpensive calcium source for nano-hydroxyapatite powder production that is useful in biomedical applications.

Keyword: African giant snail shell, Hydroxyapatite, Hydrothermal, Synthesis, Bio-ceramics, Biomedical

1. Introduction

The increasing rate of bone lesions from pathological illnesses or trauma is alarming. This represents the most common large organ injury in humans globally, posing serious threat to patients and clinicians [1]. Evidence from a statistical report in 2017 [2] indicates that up to 2.2 million bone graft procedures were done worldwide annually. There is a steady growth of 13% annually in the number of procedures for repairing bone defects in orthopaedics, dentistry and neurosurgery. Consequently, this development has ignited an enormous global market demand for bioceramic materials such as hydroxyapatites. Market demand for these materials has increased to approximately 40 billion euros per year, with an annual estimated growth rate of 7–13%. The situation that can be attributed to an increasingly aged population, healthcare expenditures and demand for medical implant-based hydroxyapatite products [2-3]. This signaled that only effective and economically sustainable bioceramic products that are readily available and accessible to all regions can meet the enormous global demand, especially in the developing countries.

Hydroxyapatite (HA) has a chemical formula of $Ca_{10}(PO_4)_6(OH)_2$ and ideal Ca/P ratio of 1.67. It is a bioceramic (bio-active and biocompatible) product that is suitable for repair and restoration of dysfunctional and diseased or defected bones [4]. It is the most prominent bio-ceramic use as bone substitute implant in lieu of autograft or allograft implant sources [5-9]. This is because of the limited supply of donors and unresolved health risks associated with autograft and allograft implant sources. However, HA can evoke non-foreign body reactions such as inflammatory or pyrogenetic responses, as well as bond strongly to the new bone tissue interface [10-11]. HA can be purchased either in pellet or powder form. It has found application in dentistry, orthopaedic prostheses, coatings for implants, drug delivery and maxillofacial applications due to its high bioactivity and osteo-conductivity properties

*Corresponding author.
Email address: maruf.kolawole@kwasu.edu.ng
doi: 10.14456/easr.2020.30

supporting bone formation with strong bone-calcium phosphate biomaterial interfaces [4, 12-14]. The powder form of HA has also been employed as a reinforcement material in a metal matrix composite for strength and bioactivity properties. These are improvements that are desirable in biomedical applications [15]. Amongst key factors that are usually considered in the synthesis of HA are processing techniques and conditions, as well as the starting materials.

Several techniques, such as sol-gel synthesis, wet methods, hydrolysis, emulsions, solid state synthesis, mechano-chemical and hydrothermal methods had been employed for the synthesis of hydroxyapatite powder. Each route has its advantages and disadvantages [4, 16]. Most common issues associated with these synthesis techniques are long reaction times, agglomeration, uncontrolled particle size and non-stoichiometric products. However, hydrothermal techniques at low or moderate temperatures with high pressures to offer good control of morphology and chemical stoichiometry, producing materials that are desired in biomedical applications [16-21]. Consequently, research interest in hydrothermal synthesis of HA is increasing and a few relevant studies are highlighted in this paper. Liu *et al.*, [22] reported on hydrothermal synthesis of $Ca(OH)_2$ and $CaHPO_4.2H_2O$ at different pH values and temperatures ranging between 6–14 and 60–140 $^{\circ}$C, respectively. This was done to investigate HA particle structure and morphology. It was discovered that pure HA cannot be formed without pH control, even at 140 $^{\circ}$C. However, increasing the synthesizing temperature with pH adjustment increases the formation of pure HA over the Monetite phase. A high ratio of HA to other forms was obtained at pH = 9 at temperature of 120 $^{\circ}$C. In a similar study [23], the influence of temperature on hydroxyapatite production from calcium carbonate single crystals via a hydrothermal technique was examined. The results showed the formation of needle-shaped HA crystals in all the samples. Additionally, the size of the HA crystals increased with hydrothermal temperature. Similar observations were reported on the characterization of hydroxyapatite nanobelts under a controlled additive-free hydrothermal technique [24]. The study concluded that hydrothermal reaction time, hydrothermal temperature, and dosage of NaOH played a critical role in the formation of HA nanobelts.

Odusote *et al*. [25] opined that production of HA from bio-waste of chicken eggshells and bovine bones, as well as coral, oyster and snail shells can constitute an important way of achieving economic and sustainable HA production. This is because the increasing human population and inter-relationship of activities in the eco-system have resulted in generation of wastes without viable economic benefit as well as posing disposal challenges, with public health and environmental threats [26-28]. Reclaiming, synthesis and conversion of inexpensive wastes such as egg, sea and snail shells into a value added HA, suggests an effective way to managing the use of large amounts of bio-wastes [27, 29-30].

African giant snail shells are the discarded shells after the removal of the fleshy portion the animal. These shells are in abundance in the southern part of Nigeria and West African sub-regions. At present, they have little or no economic value [28-29, 31]. Additionally, their indiscriminate disposal has negatively affected the well-being of the populace as well as presenting environmental pollution challenges [32-33]. Several attempts had been made to use snail shells in various applications such as catalysts [34] in biodiesel production. Jatto et al. [35] used snail shells in water treatment. Edokpayi et al. [32] used the chitosan derived from snail shells as a reinforcement in biopolymer synthesis and characterization. Adeosun et al. [12] and Odusanya et al. [36] used snail shells as a reinforcing filler in unsaturated polyester composites.

Furthermore, other researchers considered varieties of egg and snail shells as inexpensive calcium precursors for the synthesis of hydroxyapatite for biomedical applications [4, 29, 31, 37-38]. The potential utilization of Asian *Achatina achatina* snail shells as a calcium precursor for the synthesis of hydroxyapatite by chemical decomposition and in water defluoridation has been reported by Asimeng et al. [38]. It was concluded that hydroxyapatite obtained from Asian *Achatina* snail shells can serve as potential low-cost material for water fluoride removal. A similar result was reported by Kumar et al. [29] who successfully synthesized hydroxyapatite nanorods was using Indian snail shells as a calcium source. This was done via a rapid and facile microwave irradiation with EDTA as a chelating agent. In a separate report, Zhou et al. [37] prepared and characterized hydroxyapatite synthesized from Chinese mystery snail shells. The influence of condensed phosphate ions ($P_2O_7^{4-}$, $P_3O_{10}^{5}$-and $P_6O_{18}^{6-}$) as phosphate source on the properties of HA via a hydrothermal technique was examined. It was concluded that Chinese mystery snail shells could be used as alternative calcium source for preparation of hydroxyapatite with $P_6O_{18}^{6-}$ phosphate ions. These ions had a highly significant influence on HA morphology. In furtherance of biocompatibility assessment of hydroxyapatite derived from biogenic waste, HA synthesized via a sol-gel route from snail shells from an Indian river was subjected to cytotoxicity testing using NIH-3T3 cells by Anjaneyulu et al. [31]. The outcome of their investigation revealed that low cost hydroxyapatite with a 2.14 Ca/P ratio and crystallite sizes ranging from 60 – 100 nm with no cytotoxicity effect could be prepared these shell wastes. Additionally, mechanical property improvement and *in vitro* assessment of HA obtained from golden apple snail shell mixed with various weight percentages of kaolin were studied by Sutthi et al. [39]. The outcome of their experimentation revealed a peak compressive strength of 32.93 MPa for a composite of 25% hydroxyapatite and 75% calcined kaolin cured at 60 °C. Additionally, the apatite formation on sample surface after immersion in SBF for 28 days as revealed by SEM/EDS and XRD analysis indicated good bioactivity of this golden apple hydroxyapatite/kaolin derived ceramic when used as a bone substitute.

There have been a number reports on the use of different types of snail shells for hydroxyapatite preparation. However, close examination of the existing literature rarely disclosed the use of giant African land snail shell wastes for the synthesis of hydroxyapatite despite their abundance in Nigeria and other tropical regions of West Africa [12, 28]. Additionally, information on the effect of hydrothermal temperature in the preparation of hydroxyapatite from locally sourced materials is limited. Hence, this paper presents preparation and characterization of hydroxyapatite powder from waste shells of African giant land snails (*Archachatina marginata)* and compares the product with commercially available hydroxyapatite powder for potential biomedical applications.

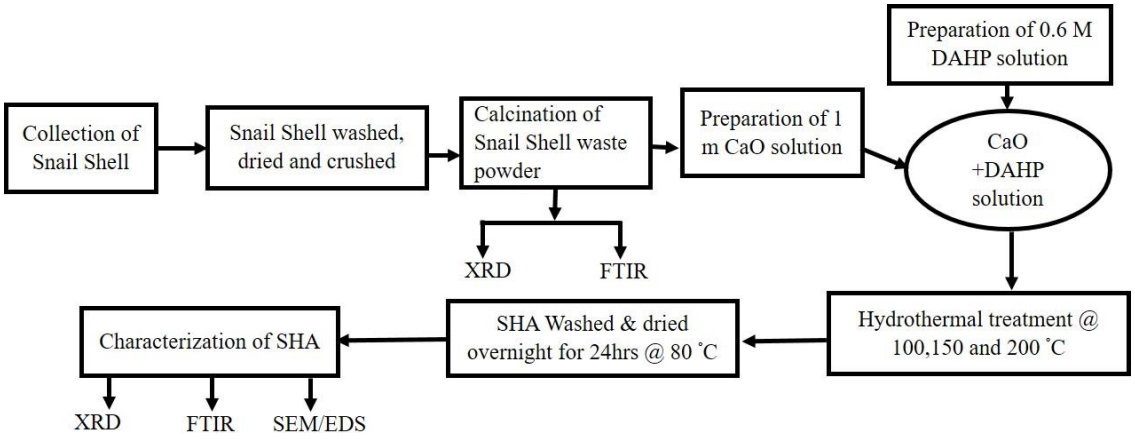

Figure 1 Process flow chart for the synthesis of hydroxyapatite powders from snail shells

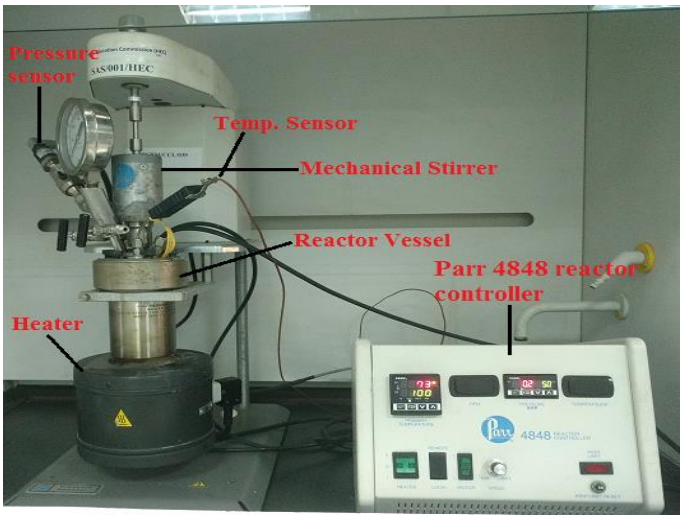

Figure 2 Hydrothermal set-up for HA synthesis

2. Materials and methods

2.1 Materials

African giant land snail shells (*Archachatina marginata)* (SnS) were collected from the Abegunde, Okitipupa Local Government, Ondo State, Nigeria. The materials were calcined to obtain a calcium oxide (CaO) that was used as calcium precursor in this study. Diammonium hydrogen phosphate ($(NH_4)_2HPO_4$, 99.0%, Cat. No. S7907) from Sigma-Aldrich, Lahore, Pakistan, was used as phosphate source. Liquid ammonia, NH_4OH, was used to adjust pH of reacting solution.

2.2 Preparation of CaO from African giant snail shell

The collected snail shells were washed using distilled water and Ariel laundry detergent to remove the hard-stuck materials. The materials were then dried in an oven at 110 ℃ for 12 hr. After that, they were crushed using a Jaw crusher and ground into powder using disc mills at the Department of Chemical Engineering, COMSATS University Islamabad, Lahore Campus, in Pakistan. A measured quantity of milled powder was then calcined with a 10 ℃/min heating rate at 900 ℃ for 3 hr in a bench top muffle furnace as reported by Kolawole et al. [28] to obtain calcium oxide (CaO), as shown in Equation 1, followed by particle size analysis. The shell powder retained on a 100 µm sieve size was used in this work. The powder was further characterized using XRF, FTIR and XRD and compared to un-calcined shell powder as discussed in Section 2.3.

$$CaCO_3 \rightarrow CaO + CO_2 \uparrow \quad (1)$$

2.3 Preparation of hydroxyapatite (HA) from snail shell wastes

The synthesized hydroxyapatite (SHA) from the snail shells was prepared following the sequence illustrated in Figure 1. A measured amount of 8.40 g of calcined snail shell powder was dissolved in 75 mL of distilled water to make a 1 M solution of CaO solution. Then, 75 mL of a 0.6 M diammonium hydrogen phosphate $(NH_4)_2HPO_4$ solution was prepared and added dropwise (40 drops/min or ~0.0417 ml/sec) using a 250 ml dropping funnel, into a prepared CaO solution while stirring at constant speed of 180 rpm for 1 hr [40]. The pH of the solution was maintained in the range of 11-12 using dropwise addition of liquid ammonia before being transferred into a hydrothermal reactor [41]. The resulting solution was then hydrothermally treated at 100, 150 or 200 ℃ for 4 hours at autogenous pressures of 0.38 bar, 4 bars and 14 bars, respectively, in a stainless-steel closed vessel reactor, as shown in Figure 2. The SHA samples obtained at various temperatures were

Table 1 Composition of Calcined S_nS using X-Ray Fluorescence (XRF)

Oxides type	NiO	Fe_2O_3	MnO	Cr_2O_3	TiO_2	CaO	Al_2O_3	MgO	ZnO	SiO_2	LOI	Total
Raw SnS	0.007	0.051	0.000	0.000		66.368	LOD	LOD	0.001	LOD	23.573	100
Calcined SnS	0	0.289	0	0.017	0	81.809	LOD	LOD	0	LOD	17.885	100

washed with de- ionized water until a neutral pH of 7 was attained. Finally, the samples were oven dried at 80 ℃ for 12 hr. The SHA powders were then characterized and compared with commercial Plasma Biotel hydroxyapatite powder (CHA).

2.4 Characterization of SnS and hydroxyapatite powder

X-ray fluorescence (XRF) analysis of both calcined and un-calcined SnS powder samples was done on pelleted samples. The X-ray fluorescence spectroscopic apparatus was operated at 30 kV to determine the chemical composition following the ASTM C114 standard procedure. Specimens of HA produced were tested on a Thermo Scientific Nicolet 6700 Fourier Transform Infrared Spectrometer within the range of 4000 - 400 cm^{-1} for 16 scans at a 4 cm^{-1} resolution to determine the functional group of the samples. Phase identifications were determined using a Philips PANalytical X'Pert Powder Diffractometer, model number PW 2050/08, employing CuKα radiation of wavelength λ = 0.1506 nm at 35 kV and 30 mA. The data were recorded in the range of 6-90^o (2θ) at a step of 0.02 and analyzed using X'Pert Highscore Plus Software. The crystallite size of both the SHA and CHA were determined using the Scherrer relationship, Equation 2, to determine the influence of hydrothermal temperatures on the crystallite size of as-prepared and commercial hydroxyapatite powders.

$$D = \frac{K\lambda}{d\cos\theta} \quad (2)$$

where "D" − crystallite diameter in Å, "k" − the shape constant (~ 0.9), "λ" − wavelength in Å (~ 1.5406), "d" − the observed peak width at half-maximum peak height in rad and "θ" − Bragg angle in degrees.

Additionally, the degree of crystallinity of both synthesized and commercial HA were obtained using Equation 3. The area of the crystalline peaks and all other peaks obtained from XRD data of the respective samples was determined using OriginPro 8.5 software. Excel were used to compute the degree of HA crystallinity.

$$Degree\ of\ crystalinity = \frac{Area\ of\ crystalline\ peaks}{Area\ of\ all\ peaks} \times 100 \quad (3)$$

A VEGAS TESCAN scanning electron microscope equipped for energy dispersive spectroscopy (EDS) was operated at a 20 kV accelerating voltage to examine the morphology and composition of HA samples. Samples for SEM observation were prepared by dispersing the powders in ethanol and immersed them in an ultrasonic bath for 5 mins. A few drops of the resulting suspension was dried in air and sputter coated with gold for SEM examination [42].

3. Results and discussion

3.1 Phase and oxide composition analysis of calcined snail shell powder

The oxide composition of African giant land snail shells calcined at 900 ℃ for 3 hours determined using X-Ray Fluorescence (XRF) analysis is presented in Table 1. This table indicates the presence of CaO as the major phase, with traces of Fe_2O_3 and Cr_2O_3. The substance loss on ignition (LOI) in Table 1 represents escape of volatile phases present in the sample due to thermal decomposition of SnS powder on ignition. Calcium oxide and carbon (IV) oxide are liberated. The analysis also showed presence of Al_2O_3, MgO and SiO_2 oxides in unquantifiable amounts, less than the limit of detection (LOD).

The XRD patterns of both calcined and un-calcined SnS are illustrated in Figure 3 with a plot of intensity versus diffraction angle. The diffraction peaks with typical values shown in Figure 3a for un-calcined shells were observed at diffraction angles (2θ) of 26.27, 33.17, 36.20, 37.9 and 45.91^o corresponding to inter-planar distances of 3.39, 2.69, 2.48, 2.37 and 1.98 Å, with relative intensity of x-ray scattering of 100, 75.38, 98.58, 45.15 and 66.76%, respectively. These peaks correspond to aragonite ($CaCO_3$) according to the JCPDS 00-041-1475 reference file. The XRD patterns of the calcined SnS powder shown in Figure 3a revealed typical diffraction peaks at 2θ values of 32.38, 37.52 and 53.99^o and inter-planar distances 2.76, 2.40 and 1.70 Å corresponding with relative intensity of x-ray scattering of 34.06, 100 and 39.85% respectively. These peaks correspond to calcia (CaO) according to the JCPDS 00-037-1497 reference file. The results clearly indicate a phase transformation of African giant land snail shell powder from aragonite into the calcia form of calcium oxide. This may be attributed to the decomposition of the highly volatile and low thermally resistant constituents of the un-calcined shell to a thermally stable calcia (CaO) obtained during the calcination process. This is similar and in agreement with that reported earlier [30]. This implies that, un-calcined SnS powder mainly contains calcium carbonate and calcination can transformed the raw SnS powder to calcium oxides. Hence, Figure 2 confirms that both un-calcined (Figure 3b) and calcined (Figure 3c) SnS powders are in absolute agreement with the reference material due to correct matching of the spectrum as revealed by X'Pert Highscore XRD analysis software.

It can be inferred that in the presence of aragonite ($CaCO_3$) as the main phase, SnS may be responsible for the hard nature of the African giant land snail shells. When fired at 900 ^{o}C for 3 hours, it was noticed that the aragonite minerals decomposed through calcination to yield calcia (CaO) as the sole major phase. This means that aragonite is presumed to be thermodynamically unstable when subjected to elevated temperatures and it will transform into thermodynamically stable hard phases (calcia, CaO) at 900 ℃ with the evolution of CO_2 and other volatile constituents.

3.2 Fourier Transform Infrared (FTIR) analysis of calcined and un-calcined SnS powder

FTIR Spectra analysis of both calcined and un-calcined SnS powder, illustrated in Figure 4, shows two main functional groups in both samples. The water bands observed at 3641.9 cm^{-1} and 660.07 cm^{-1} in calcined SnS powder and 705.93 cm^{-1} in un-calcined powder were due to stretching and liberation of the hydrogen bonds of OH^- ions, respectively.

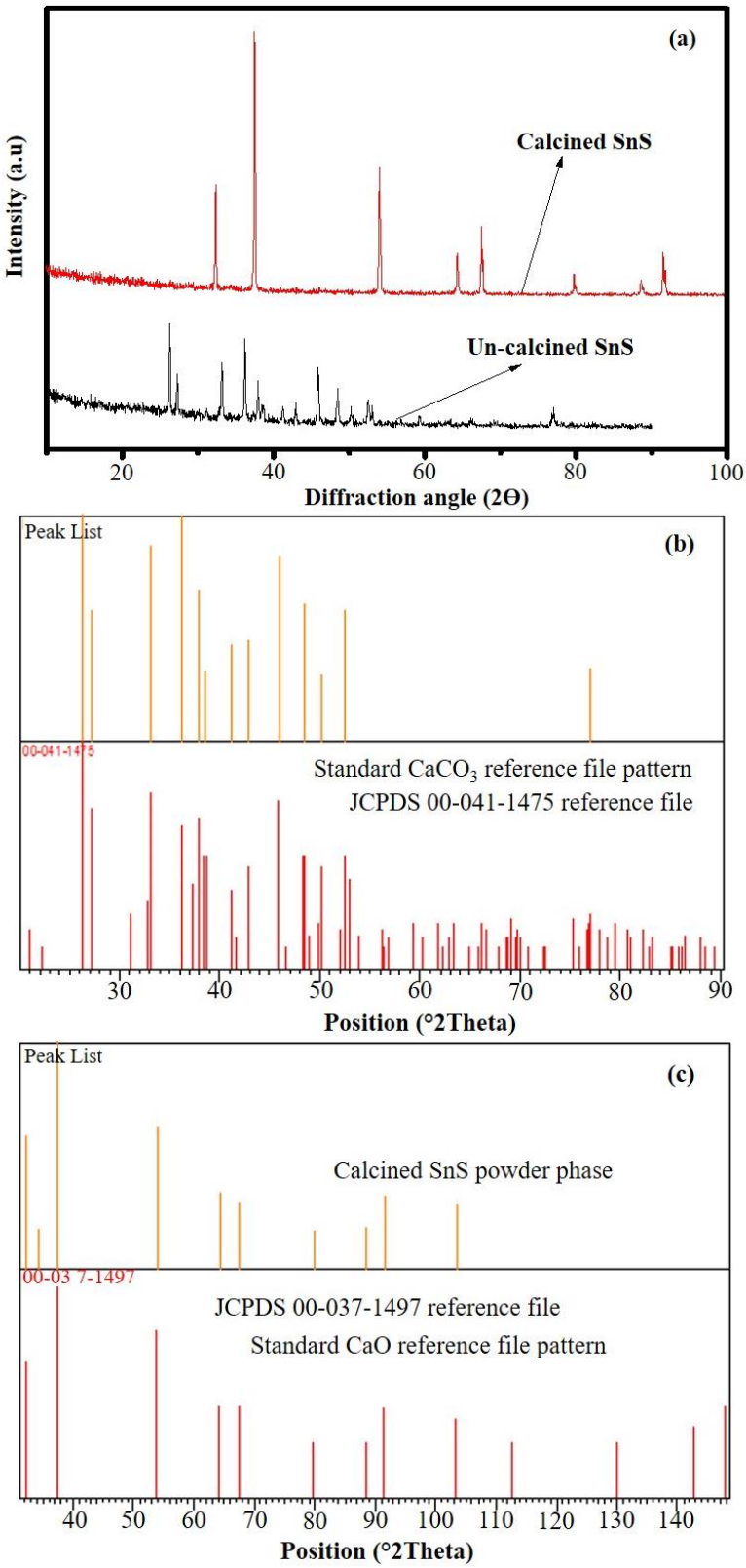

Figure 3 XRD patterns of (a) calcined and un-calcined SnS powder and XRD reference pattern for un-calcined, (b) calcined and (c) SnS powder

The CO_3^- band peaks at 1426.08 and 871.94 cm^{-1} of calcined SnS powder were low in intensity due to loss of CO_2 from thermal decomposition to yield a high amount of calcium oxide [30]. Additionally, the CO_3^- band peaks observed in un-calcined SnS samples were found at around 863, 1454 and 1777 cm^{-1}. The carbonate groups were from calcium carbonate in snail shells. It can be noted that, the carbonate peaks in the un-calcined sample were higher and characterized by high intensity compared with the calcined sample. This shows that during the calcination process,

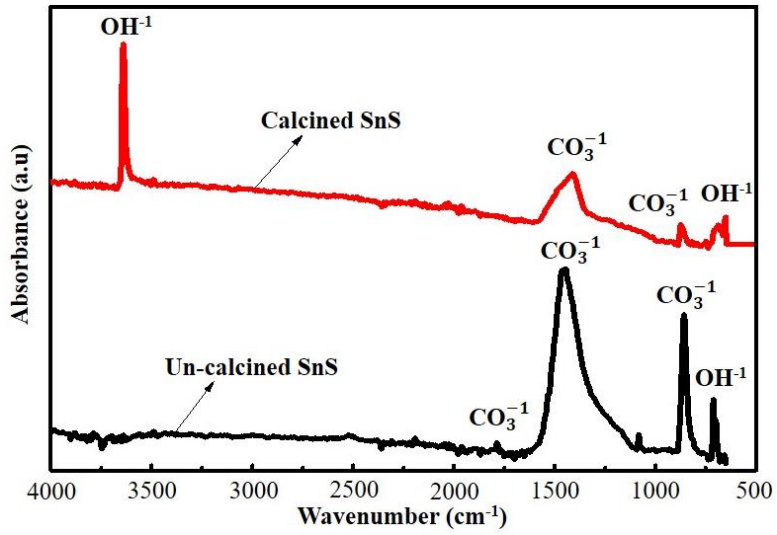

Figure 4 FTIR spectra analysis of calcined and un-calcined SnS powders

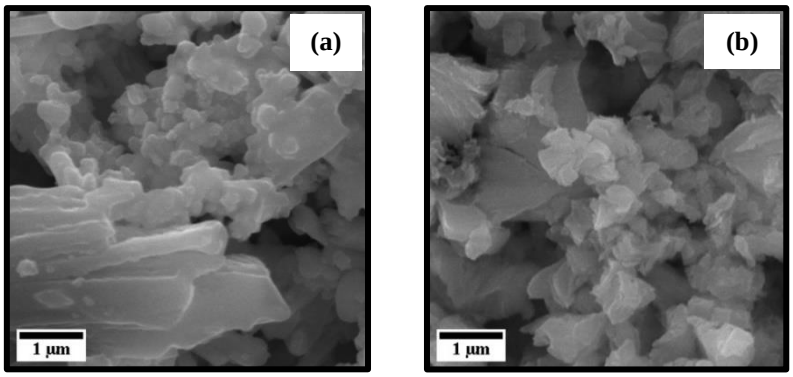

Figure 5 SEM of (a) un-calcined and (b) calcined snail shell powders

most of the carbonate in the shell sample was decomposed due to the very high temperature involved. The high peak of OH^- may be attributed to the deliquescent nature of CaO, which was exposed to the atmosphere probably during the test. This implies that calcination of SnS at 900 ℃ for 3 hr of soaking time was adequate for the synthesis of CaO from snail shells. Nevertheless, traces of carbonate were detected as indicated by presence of CO_3^- in the calcined samples. This could be due to adsorption of H_2O and CO_2 by CaO during storage as depicted by Equation 4.

$$CaO \longrightarrow Ca(OH)_2 \longrightarrow CaCO_3 \quad (4)$$

3.3 SEM analysis of un-calcined and calcined African giant land snail shell powders

The microstructure of un-calcined and calcined SnS powders is presented in Figure 5. Un-calcined SnS powder was characterized by mixtures of irregular and elongated platelet rod-like shaped grains with an average size of 0.4 µm as determined using image J software. The calcined SnS powder microstructure presented smaller equiaxed grains with an average size of 0.0003 µm compared to un-calcined powder, 0.4 µm. The elongated platelet grains of un-calcined powder display a characteristic feature of calcium carbonate structures. When calcined, the platelet rod-like structures decomposed into smaller fused grains due to high temperature coupled with the associated sintering effects. The smaller equiaxed grains of calcined particles can enhance material performance when incorporated as a reinforcement in a metal matrix for strengthening.

3.4 Characterization of hydroxyapatite powder

3.4.1 Fourier Transform infrared (FTIR) analysis of hydroxyapatite powder (HA)

Fourier Transform Infrared analysis was done of hydroxyapatite powders produced at different temperatures (100, 150 and 200) ℃ and denoted as SHA100, SHA150, and SHA200, respectively. These powders, as well as a commercial Plasma Biotel hydroxyapatite powder (CHA), exhibit similar spectral patterns for both the synthesized hydroxyapatite at different temperatures with no notable differences. The FTIR results are presented in Figure 6. It can be deduced that hydrothermal synthesis temperature has no effect on the functional groups of hydroxyapatite powder. The characteristic frequencies derived from PO_4^- modes are conspicuously seen with strong intensities at around 964, 1019, 1045 cm^{-1} bands, thus confirming the successful formation of hydroxyapatites. A very weak broad band spectrum observed around 1430 and 1450 cm^{-1} indicates traces of the stretching mode of CO_3^{2-} in all

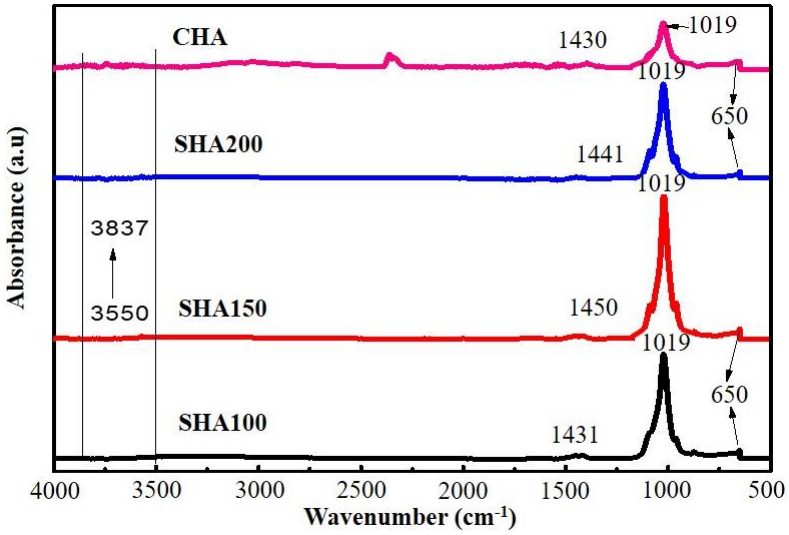

Figure 6 FTIR analysis of SHA at varying temperatures compared with CHA powders

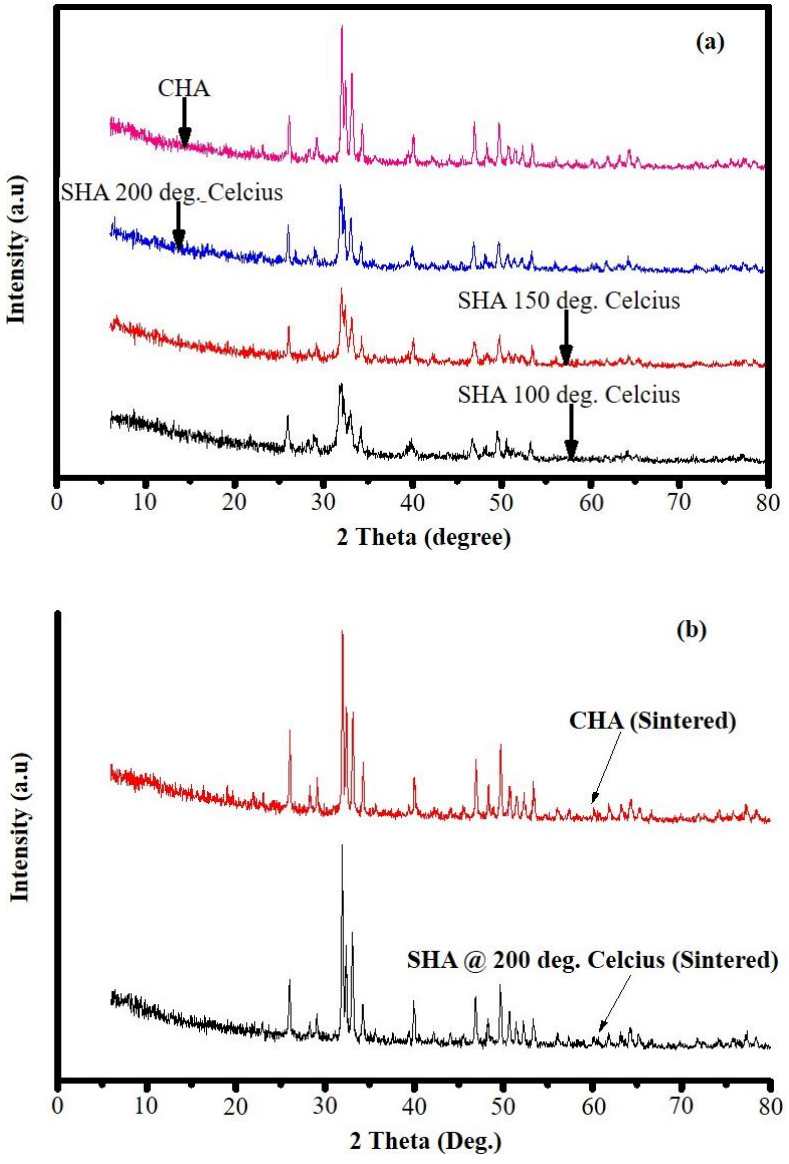

Figure 7 XRD pattern of synthesized and commercial hydroxyapatite powders

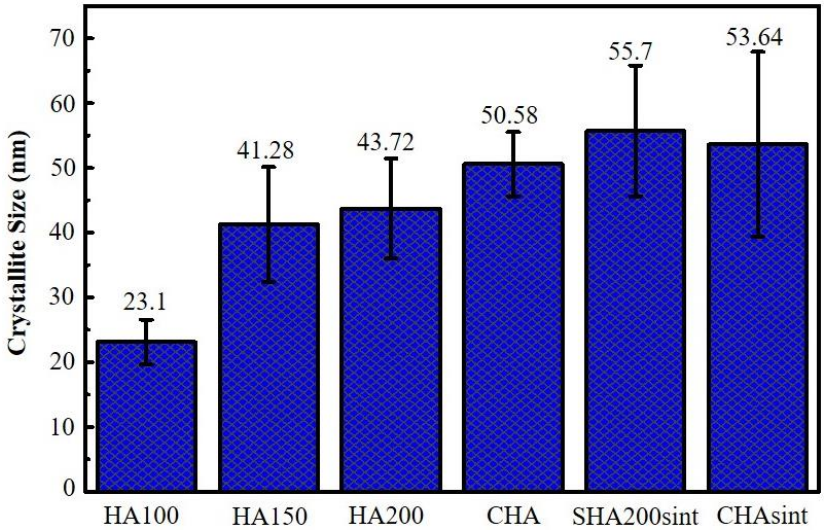

Figure 8 Influence of synthesis temperature on the crystallite size of hydroxyapatites

Table 2 Degree of crystallinity of hydroxyapatites

Parameters	SHA100	SHA150	SHA200	CHA	SHA200-sintered	CHA-sintered
Sum of crystalline peaks	555.6745	624.1801	639.1337	775.9644	689.493	779.6626
Area of all peaks	669.153	682.458	695.0195	852.231	740.214	805.565
Degree of crystallinity (%)	**83**	**91**	**92**	**91**	**93**	**97**

samples, including the CHA sample. The presence of CO_3^{2}, though very minimal in samples of synthesized HA, may be as a result of using CaO derived from snail shells or from an equipment calibration error. The bands at 3550 and 3837 cm^{-1} are due to adsorbed water associated with structural OH^- in HA. The bending band due to the structural OH^- in SHA also occurs at 650 cm^{-1} in all samples. These observations and results agree with the earlier works of [4, 43-45] where hydroxyapatite powder was produced from biogenic wastes.

3.4.2 XRD studies of synthesized and commercial hydroxyapatite powder

X-ray diffraction spectra of both the CHA and SHA powders are showed in Figure 7(a). They indicate that the XRD peaks pattern for hydroxyapatite powders prepared at various temperatures and commercial hydroxyapatite samples were similar. A marginal change in the crystallinity with increased synthesis temperature was noticed in SHA compared to the CHA sample having the highest crystallinity. The samples were characterized by strong and narrow intensities peaks. However, in all SHA samples, the patterns indicated the presence of highly crystalline hydroxyapatite with major peaks at 26.085, 31.8, 32.44 and 33.15^o (2θ). These patterns are in good agreement with JCPDS reference number (00-009-0432) for hydroxyapatite. No characteristic peaks of impurities, such as calcium hydroxide and calcium phosphates, were observed. This implies that pure or single-phase HA was successfully prepared under the present experimental conditions. Similar results were obtained after sintering the as-prepared SHA and CHA powders. Though an increase in crystallinity was indicated by sharper and longer peak patterns, as depicted in Figure 7 (b), it was observed in both sintered samples, in agreement with earlier reports [27, 46].

Figure 8 illustrates and compares the influence of hydrothermal synthesis temperatures on the crystallite size of produced hydroxyapatites and commercial HA. It was observed that the crystallite size of SHA increases with synthesis temperature. This implies that increasing the hydrothermal temperature favours crystal growth of hydroxyapatites. It is noteworthy that at hydrothermal synthesis temperatures of 100, 150 and 200 ^oC, the crystallite resulting sizes were 23, 41 and 44 nm, respectively, while it was 51 nm for commercial hydroxyapatite. Moreover, when hydroxyapatite prepared at 200 ℃ and commercial hydroxyapatite powder were sintered at 900 ^oC for 1 hr to avoid phase transformation [27, 47], it was observed that the crystallite size increased to 56 and 54 nm, respectively. Comparing this outcome with previous results [31, 37], the average particle size of HA synthesized were in the range of 60 – 100 nm [31] and 10-15 nm wide and 50 – 100 nm long [37]. This implies that, the present study produced a better nano-crystalline HA structure from giant African land snail shells. These differences may have been a result of some variation in materials and processing parameters used in the synthesis. Concurrently, the degree of crystallinity, as depicted in Table 2, also increased with hydrothermal temperature. It is noteworthy that the degree of crystallinity of SHA100, SHA150, SHA200 and CHA were 83, 91, 92 and 91%, respectively, which further increased to 93 and 97% for SHA200 and CHA, respectively, when sintered at 900 ^oC. This implies that both crystallite size and crystallinity are a function of temperature. The increase in crystallite size and crystallinity can be attributed to elevated hydrothermal process temperature and sintering, which support grain growth. These results are in agreement with earlier reports [46, 48] attributing crystallite growth to increased temperature and time.

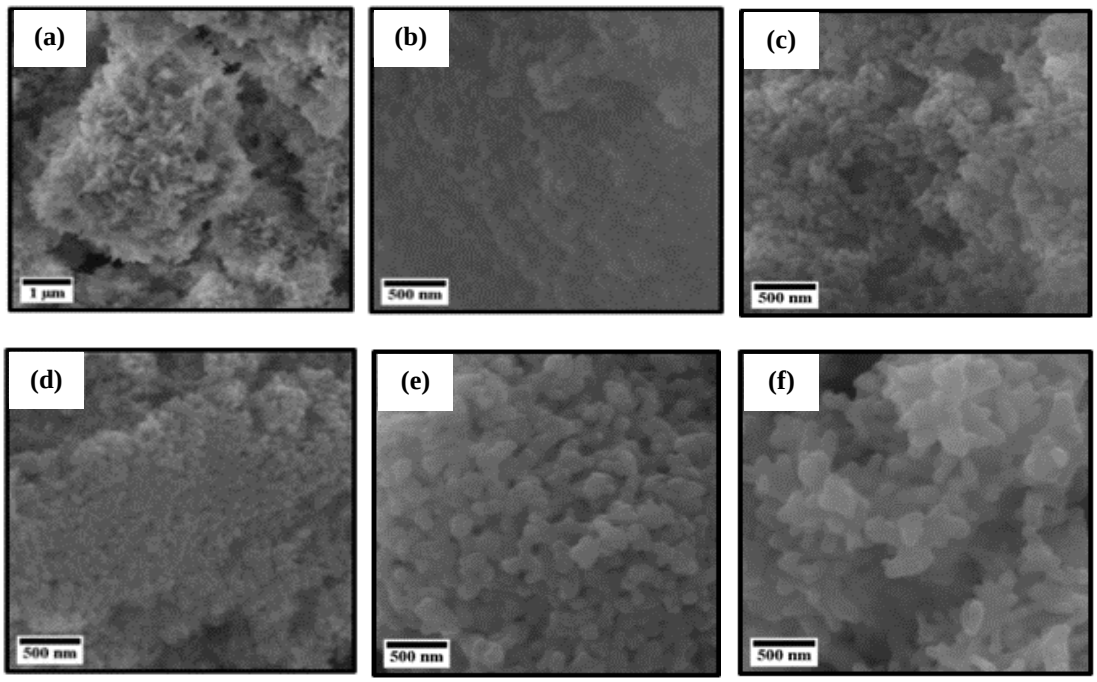

Figure 9 Microstructure of (a) commercial hydroxyapatite (CHA), (b-d) synthesized hydroxyapatite (SHA) at 100, 150 and 200 ℃, respectively, and (e-f) sintered SHA200 and CHA, respectively

Table 3 Elemental composition of synthesized, commercial and sintered hydroxyapatite

Sample ID	Composition (at. %)				Stoichiometry
	C	O	Ca	P	Ca/P
CHA	16.09	58.02	15.14	10.74	1.41
SHA100	14.73	62.32	14.14	8.82	1.60
SHA150	13.33	59.27	17.56	9.85	1.78
SHA200	11.98	63.49	14.55	9.98	1.46
Sintered CHA	14.39	58.11	16.71	10.78	1.55
Sintered SHA200	21.38	55.68	13.84	9.10	1.52

3.4.3 Morphological and compositional analysis of hydroxyapatite powder

The morphologies of synthesized and commercial hydroxyapatite powders were examined using scanning electron microscopy (SEM)/energy dispersive spectroscopy (EDS). The results are presented in Figure 9. A nanostructural rice-like morphology was observed in HA synthesized at 100 ℃ (Figure 9b). This morphology conspicuously increases in size as the synthesis temperature increases from 100 to 200 ℃ (Figure 9c-d). The increase in particle size can be attributed to diffusion of the HA crystal particles at elevated temperatures over time and grain growth [48]. For un-sintered commercial hydroxyapatite powder, a nano-size flaky structure was observed that was fused and difficult to differentiate (Figure 9a). Figures 9e and 9f show structural transformation of the synthesized and commercial HA which form a rice-like or flake like structure into one with an interconnected porous rod flake-like morphology after sintering at 900 ℃ under the same conditions. This characteristic feature may have been due to the diffusion of the particles at higher temperatures and formation of flake-like structures with interconnections as reported earlier [27, 49-50]. The porous nature of these morphologies can also be an advantage to support the growth of new bone during the regeneration process. The SEM/EDS results of both commercial and synthesized HA at various temperatures with Ca, P and O_2 forming the basic elemental composition at similar levels are shown in Table 3. However, the presence of carbon was seen in the EDS results in all samples, even the commercial hydroxyapatite. Carbon may, however, be attributed to equipment calibration error and absorbed carbonate (CO_3^-) while obtaining calcium oxide from SnS. This was observed in the FTIR results (Figure 6) of calcined snail shells [13]. The calcium to phosphate ratio (Ca/P) in all samples was evaluated from EDS results because of its strong influence on the mechanical strength and biodegradation of HA [49, 51-52]. The Ca/P ratios were 1.60, 1.78 and 1.46 as the hydrothermal temperature increased from 100 to 200 ℃. Commercial hydroxyapatite had a Ca/P ratio of 1.41. This result shows that SHAs has an improved Ca/P ratio compared to CHA. Ca/P HA ratios of 1.26 -1.33 were reported by Zhou et al. [37], which are close to that of ideal HA, a Ca/P ratio of 1.67. When HA prepared at 200 ℃ and commercial HA powder were sintered at 900 ℃, the (Ca/P) ratio increased from 1.46 to 1.52 and from 1.41 to 1.46, respectively. This translates to molar ratios equivalent to 4.1 and 3.5%, respectively. Such a marginal increase may be attributed to heating during sintering where some volatile substances may escape and increased dissolution of the CaO precursor in the diammonium hydrogen/CaO slurry solution to yield the increased Ca/P ratio observed in this study. This finding suggests that sintering may increase the Ca/P ratio. However, care must be taken in selection of an appropriate

temperature to avoid the formation of unwanted phases. This result is in agreement with the work of earlier authors [13, 27, 52-54], where an increased Ca/P ratio was reported with increased synthesis temperatures between 160 to 200 ℃.

4. Conclusions

This study presents the synthesis and characterization of hydroxyapatite powders obtained from waste shells of giant African snails (*Archachatina marginata)*. The process was a hydrothermal technique at three different temperatures (100, 150 and 200 ℃). Our study compared the samples that we synthesized to commercially available hydroxyapatite powder. The following specific conclusions are offered:

i. A calcium oxide phase with a 81.8% yield was obtained from calcination of SnS powder at 900 ºC with 3 hours of soaking time, relative to 66.4% CaO in un-calcined SnS.
ii. Nano-hydroxyapatite powder with 23.10 to 43.73 nm crystallite sizes was successfully prepared using giant African snail shells (*Archachatina marginata*) under temperatures ranging from 100 to 200 °C using a hydrothermal technique.
iii. The hydrothermal synthesis temperature influenced the crystal size and microstructure of the prepared hydroxyapatite powder. A minimum crystallite size of 23.1 nm with a good Ca/P stochiometric ratio of 1.6 was closer to ideal HA of 1.67. A material suitable for biomedical application was obtained using a 100 °C hydrothermal process temperature as compared to a 50.58 nm crystal size for commercial hydroxyapatite powder.
iv. The XRD, FTIR analyses and Ca/P ratios of 1.60 – 1.78 for hydroxyapatite powder prepared from giant African snail shells matched commercially available HA. Hence, giant African snail shells can be considered an alternative calcium source for preparation of hydroxyapatite powder produced at 100 °C that is suitable for biomedical applications.

5. Future work

The bioactivity properties tests of SHA using giant African snail shell (*Archachatina marginata)* as a calcium precursor will be examined in further studies for complete characterization

6. Acknowledgement

The author acknowledges the World Academy of Science (TWAS) and the Interdisciplinary Research Centre on Biomedical Material, Comsat University Islamabad, Lahore Campus, Pakistan, for the grant of a Ph. D. Research Fellowship and provision of the facilities used in this research work, respectively.

7. References

[1] Granito RN, Renno AC, Yamamura H, de Almeida MC, Ruiz PL, Ribeiro DA. Hydroxyapatite from fish for bone tissue engineering: a promising approach. Int J Mol Cell Med. 2018;7(2):80-90.
[2] Ratnayake JT, Mucalo M, Dias GJ. Substituted hydroxyapatites for bone regeneration: A review of current trends. J Biomed Mater Res B Appl Biomater. 2017;105(5):1285-99.
[3] Zaits AV, Golovanova OA, Kuimova MV. Study of the effects of heat-treatment of hydroxyapatite synthesized in gelatin matrix. IOP Conf Ser Mater Sci Eng. 2017;168:1-6.
[4] Teerawat L. Synthesis of hydroxyapatite from biogenic wastes. KKU Eng J. 2015;42(3):269-75.
[5] Chena QZ, Wongb CT, Lub WW, Cheungb KMC, Leongb JCY, Luk KDK. Strengthening mechanisms of bone bonding to crystalline hydroxyapatite in vivo. Biomaterials. 2004;25:4243-54.
[6] Jaber HL, Hammood AS, Parvin N. Synthesis and characterization of hydroxyapatite powder from natural Camelus bone. J Aust Ceram Soc. 2018;54: 1-10.
[7] Manafi S, Mirjalili F, Reshadi R. Synthesis and evaluation of the bioactivity of fluorapatite–45S5 bioactive glass nanocomposite. Progr Biomater. 2019;8:77-89.
[8] Sheikh Z, Hamdan N, Ikeda Y, Grynpas M, Ganss B, Glogauer M. Natural graft tissues and synthetic biomaterials for periodontal and alveolar bone reconstructive applications: a review. Biomater Res. 2017;21:1-20.
[9] Wang M. Developing bioactive composite materials for tissue replacement. Biomaterials. 2003;24:2133-51.
[10] Oh S, Son JS, Kim JM, Appleford M, Ong JL, Choi SH. Repair of large segmental bone defect using hydroxyapatite/alumina bi-layered scaffold with Isotropicized-pore structures. The Orthopaedic Research Society (ORS) 2011 Annual Meeting; 2011 Jan 13-16; Lomng Beach, California. p. 1.
[11] Wang W, Yeung KW. Bone grafts and biomaterials substitutes for bone defect repair: a review. Bioact Mater. 2017;2(4):224-47.
[12] Adeosun SO, Akpan EI, Akanegbu HA. Thermo-mechanical properties of unsaturated polyester reinforced with coconut and snail shells. Int J Compos Mater. 2015;5(3):52-64.
[13] Hamidi AA, Salimi1 MN, Yusoff AHM. Synthesis and characterization of eggshell-derived hydroxyapatite via mechanochemical method: a comparative study. AIP Conf Proc. 2017;1835(1):1-12.
[14] Chandran P, Azzabi M, Miles J, Andrews M, Bradley J. Furlong hydroxyapatite-coated hip prosthesis versus the Charnley cemented hip prosthesis. J Arthroplasty. 2010;21(2):52-7.
[15] Stüpp CA, Szakács G, Mendis CL, Gensch F, Müller S, Feyerabend F, et al. Powder metallurgical synthesis of biodegradable Mg-hydroxyapatite composites for biomedical applications. In: Manuel MV, Singh A, Alderman M, Neelameggham NR, editors. Magnesium Technology. Cham: Springer; 2015. p. 425-9.
[16] Onur RB, Caner D. Hydrothermal synthesis of hydroxyapatite from calcium sulfate hemihydrate. Am J Biomed Sci. 2012;4(1):50-9.
[17] Earl JS, Wood DJ, Milne SJ. Hydrothermal synthesis of hydroxyapatite. J. Phys Conf Ser. 2006;26:268-71.
[18] Fujishiro Y, Yabuki H, Kawamura K, Sato T, Okuwaki A. Preparation of needle-like hydroxyapatite by homogeneous precipitation under hydrothermal conditions. J Chem Tech Biotechnol. 1993;57(4):349-53.
[19] Guijun Y, Soo-Jin P. Conventional and micro-wave hydrothermal synthesis and application of functional materials: a review. Materials. 2019;12(7):1-18.

[20] Wang Y, Zhang S, Wei K, Zhao N, Chen J, Wang X. Hydrothermal synthesis of hydroxyapatite nanopowders using cationic surfactant as a template. Mater Lett. 2006;60(12):1484-7.
[21] Yoshimura M, Suda H. Hydrothermal processing of hydroxyapatite: past, present, and future. In: Brown PW, Constantz B, editors. Hydroxyapatite and related compounds. Boca Raton: CRC Press; 1994. p. 45-72.
[22] Liu J, Ye X, Wang H, Zhu M, Wang B, Yan H. The influence of pH and temperature on the morphology of hydroxyapatite synthesized by hydrothermal method. Ceram Int. 2003;29(6):629-33.
[23] Kim IY, Ohtsuki C. Hydroxyapatite formation from calcium carbonate single crystal under hydrothermal condition: effects of processing temperature. Ceram Int. 2016;42(1):1886-90.
[24] An L, Li W, Xu Y, Zeng D, Cheng Y, Wang G. Controlled additive-free hydrothermal synthesis and characterization of uniform hydroxyapatite nanobelts. Ceram Int. 2016;42(2):3104-12.
[25] Odusote JK, Danyuo Y, Baruwa AD, Azeez AA. Synthesis and characterization of hydroxyapatite from bovine bone for production of dental implants. J Appl Biomater Funct Mater. 2019;17(2):1-7.
[26] Gaby RM, Pierre FE. Use of crushed seashell by-products for sandy subgrade stabilization for pavement purpose. Editors. 14th LACCEI International Multi-Conference for Engineering, Education, and Technology; 2016 Jul 20-22; San José, Costa Rica. p. 1-7.
[27] Khiri MZ, Matori KA, Zaid MH, Abdullah CA, Zainuddin N, Alibe IM, et al. Crystallization behavior of low-cost biphasic hydroxyapatite/β-tricalcium phosphate ceramic at high sintering temperatures derived from high potential calcium waste sources. Results Phys. 2019;12:638-44.
[28] Kolawole MY. Aweda JA, Abdulkareem S. Archachatina marginata bio-shells as reinforcement material in metal matrix composites. Int J Automot Mech Eng. 2017;14(1):4068-79.
[29] Kumar GS, Sathish L, Govindan R, Girija EK. Utilization of snail shells to synthesize hydroxyapatite nanorods for orthopedic applications. RSC Adv. 2015;5:39544-8.
[30] Sarute U, Benchamaporn T. Utilization of eggshell waste as raw material for synthesis of hydroxyapatite. Colloid Polymer Sci. 2015;293:2477-83.
[31] Anjaneyulu U, Pattanayak DK, Vijayalakshmi U. Snail shell derived natural hydroxyapatite: effects on NIH-3T3 cells for orthopedic applications. Mater Manuf Process. 2016;31(2):206-16.
[32] Edokpayi JN, Odiyo JO, Popoola EO, Alayande OS, Msagati TA. Synthesis and characterization of biopolymeric chitosan derived from land snail shells and its potential for Pb2+ removal from aqueous solution. Materials. 2015;8(12):8630-40.
[33] Jatto OE, Asia IO, Medjor WE. Proximate and mineral composition of different species of snail shell. Pac J Sci Tech. 2010;11(1):416-9.
[34] Sani J, Samir S, Rikoto II, Tambuwal AD, Sada A, Mairhanu SM, et al. Production and characterization of heterogeneous catalyst (CaO) from snail shell for biodiesel production using waste cooking oil. Innov Ener Res. 2017;6(2):1-4.
[35] Jatto EO, Asia IO, Egbon EE, Otutu JO, Chukwuedo ME, Ewansih CJ. Treatment of waste water from food industry using snail shell. Academia arena. 2010; 2(1):32-6.
[36] Odusanya AA, Bolasodun B, Madueke CI. Property evaluation of hybrid seashell/snail shell filler reinforced unsaturated polyester composite in comparison with seashell and snail shell filler reinforced unsaturated polyester composite. Int J Eng Sci. 2014;3(12):80-90.
[37] Zhou H, Yang M, Zhang M, Hou S, Kong S, Yang L, et al. Preparation of Chinese mystery snail shells derived hydroxyapatite with different morphology using condensed phosphate sources. Ceram Int. 2016;42(15):16671-6.
[38] Asimeng BO, Fianko JR, Kaufmann EE, Tiburu EK, Hayford CF, Anani PA, et al. Preparation and characterization of hydroxyapatite from Achatina snail shells-effect of carbonate substitution and trace elements on defluoridation of water. J Asian Ceram Soc. 2018;6(3):205-12.
[39] Sutthi R, Pangdaeng S, Chindaprasirt P, Otsuka Y, Mutoh Y, Laonapakul T. Hydroxyapatite from golden apple snail shell with calcined kaolin for biomaterial applications. Key Eng Mater. 2017;718:133-8.
[40] Ganachari SV, Bevinakatti AA, Yaradoddi JS. Rapid synthesis, characterization, and studies of hydroxyapatite nanoparticles. Adv Mater Sci Res. 2016;1(1):9-13.
[41] Bundela H, Bajpai AK. Designing of hydroxyapatite-gelatin based porous matrix as bone substitute: Correlation with biocompatibility aspects. Express polym Lett, 2008;2(3):201-13.
[42] Martínez-Castañón GA, Loyola-Rodríguez JP, Zavala-Alonso NV, Hernández-Martínez SE, Niño-Martínez N, Ortega-Zarzosa G, et al. Preparation and characterization of nanostructured powders of hydroxyapatite. Superficies y vacío. 2012;25(2):101-5.
[43] Gergely G, Wéber F, Lukács I, Illés L, Tóth AL, Horváth ZE, et al. Nano-hydroxyapatite preparation from biogenic raw materials. Cent Eur J Chem. 2010;8(2):375-81.
[44] Rani DP, Yusril Y. Preparation and characterization of hydroxyapatite based on human teeth with various calcination. 2018 1st International conference on bioinformatics, biotechnology and biomedical engineering; 2018 Oct 19-20; Yogyakarta, Indonesia. USA; IEEE; 2018. p. 1-4.
[45] Saheed AM, Hassan RA, Thajeel, KM. Synthesis of calcium hydroxyapatite powder from hen's eggshell. Iraqi J Phys. 2011;9(16):24-8.
[46] Ito N, Kamitakahara M, Murakami S, Watanabe N, Ioku K. Hydrothermal synthesis and characterization of hydroxyapatite from octacalcium phosphate. J Ceram Soc Japan. 2010;118(1380):762-6.
[47] Monmaturapoj N, Yatongchai, C. Effect of sintering on microstructure and properties of hydroxyapatite produced by different synthesizing methods. J Met Mater Miner. 2010;20(2):53-61.
[48] Rodrı´guez-Lugo V, Karthik TVK, Mendoza-Anaya D, Rubio-Rosas E, Villasen˜or Cero´n LS, Reyes-Valderrama MI, et al. Wet chemical synthesis of nanocrystalline hydroxyapatite flakes: effect of pH and sintering temperature on structural and morphological properties. R Soc Open Sci. 2018;5(8):1-14.
[49] Fathi MH, Hanifi A, Mortazavi V. Preparation and bioactivity evaluation of bone-like hydroxyapatite nanopowder. J Mater Process Tech. 2008;202(1-3):536-42.

[50] Rhee SH. Synthesis of hydroxyapatite via mechanochemical treatment. Biomaterials. 2002;23 (4):1147-52.
[51] Khandelwal H, Prakash S. Synthesis and characterization of hydroxyapatite powder by eggshell. J Miner Mater Char Eng. 2016;4(2):119-26.
[52] Ramesh S, Tan CY, Hamdi M, Sopyan I, Teng WD. The influence of Ca/P ratio on the properties of hydroxyapatite bio-ceramics. International Conference on Smart Materials and Nanotechnology in Engineering; 2007 Jul 1-4; Harbin, China. USA: SPIE; 2007. p. 1-6.
[53] Jinawath S, Pongkao D, Yoshimura M. Hydrothermal synthesis of hydroxyapatite from natural source. J Mater Sci Mater Med. 2012;13:491-4.
[54] Resmim CM, Dalpasquale M, Vielmo NI, Mariani FQ, Villalba JC, Anaissi FJ, et al. Study of physico-chemical properties and in vitro antimicrobial activity of hydroxyapatites obtained from bone calcination. Progr Biomater. 2019;8:1-9.